Solar Energy Materials & Solar Cells 250 (2023) 112094

Contents lists available at ScienceDirect

Solar Energy Materials and Solar Cells

journal homepage: www.elsevier.com/locate/solmat

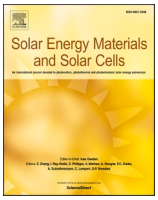

Interplay between Li and Na amid co-doped solution-processed $Cu_2ZnSn(S,Se)_4$ absorbers for solar cells

S. Moser *, A.N. Tiwari, R. Carron

Laboratory for Thin Films and Photovoltaics, Empa - Swiss Federal Laboratories for Materials Science and Technology, Überlandstrasse 129, 8600, Dübendorf, Switzerland

ARTICLE INFO

Keywords:
Solar cell
Thin films
Kesterite
CZTSSe
Doping
Alloying

ABSTRACT

Alkali doping and alloying are well-known strategies to improve the performance of $Cu_2ZnSn(S,Se)_4$ (CZTSSe) absorber based thin film solar cells. The effects of individual light alkali elements such as Li and Na have been thoroughly investigated, with both dopants resulting in significant improvements in performance of CZTSSe solar cells. Here, the combined effects of Li and Na are investigated in a so-called co-doping approach to capture the benefits from both elements simultaneously. In order to do that, various concentrations of Li and Na between 0.0 M and 0.5 M are added to the solution used for spin coating of the precursor layer. After annealing under Se-enriched atmosphere, the two alkali elements displayed mutual dependency in terms of their concentrations in the CZTSSe absorber layer. Furthermore, both, Li and Na showed signs of forming alloys with the CZTSSe phase. The efficiencies of the best Li–Na co-doped solar cells are above 10%, slightly above the Li baseline thanks to increased open-circuit-voltage and short-circuit current. A non-negligible Na incorporation was observed even in nominally Na-free devices, likely from indirect contamination from the SLG substrate. Further work is needed to better understand Na-poor compositions and draw conclusions relevant to Na-free substrates.

1. Introduction

Solar cells made from $Cu_2ZnSn(S,Se)_4$ (CZTSSe) absorber material are of considerable interest due to their composition out of earth-abundant and non-toxic elements. Yet, the power conversion efficiency of such devices has not got beyond 13.6% so far [1]. It is understood that low defect formation energy – for vacancies, interstitials, antisites and/or defect clusters – sets the limit mainly reflecting in a substantial open-circuit voltage (V_{oc}) deficit [2–5]. Doping and alloying using alkali elements has been demonstrated to reduce the V_{oc} deficit, with Haass et al. reporting Li and Na being the most effective alkali elements for CZTSSe absorbers [6].

Xin et al. demonstrated in 2015 that Li doping improves conductivity in the absorber layer and that the electrical potential at the grain boundaries (GB) can be inverted. The latter then leads to upward band bending and thus reduced recombination by repelling minority carriers [7]. If Li is added in larger amounts, it can be incorporated into the lattice, predominantly occupying Cu-sites [2,8]. The capability of Li occupying Cu-sites in the CZTSSe lattice stems from its similar ionic radius compared to Cu and hence low formation energy of substitutional Li_{Cu} defect [2,9]. Occupation of lattice sites by Li is referred to as Li-alloying leading to $(Li_xCu_{1-x})_2ZnSn(S,Se)_4$ (LCZTSSe) compounds. The kesterite crystal structure can be preserved up to a group-I element ratio [Li]/([Li]+[Cu]) = 0.4. At higher ratios, a miscibility gap is reached before a change to the wurtz-kesterite structure occurs above [Li]/([Li]+[Cu]) = 0.6 [8]. It was demonstrated that Li-alloying, on the one hand, widens the band gap, so that controlling the [Li]/([Li]+[Cu]) ratio allows to tune the band gap of CZTSSe absorbers. On the other hand, it increases the lattice parameter *a* as a result of different bond valence parameters of Li-Se and Cu–Se [10]. Furthermore, an improvement in morphology – attributed to the formation of fluxing agent Li_xSe during annealing – an increase in apparent carrier concentration and improved crystallization were observed upon Li-alloying [8,11,12]. Cabas Vidani et al. reported a LCZTSSe-based champion device with a power conversion efficiency of 11.6% [12].

Doping with Na, on the other hand, increases grain sizes and improves morphology reportedly via the formation of the low-temperature Na_xSe fluxing agent [2,13]. Furthermore, the optoelectronic properties are improved upon Na doping due to an increase in hole concentration and passivation of non-radiative defects [2,5,13–16]. This is based on the occupation of Cu-sites by Na preventing the formation of Zn_{Cu} shallow donor defects [4,14]. The crystal structure of $(Na_xCu_{1-x})_2ZnSn$

* Corresponding author.
E-mail address: simon.moser@empa.ch (S. Moser).

https://doi.org/10.1016/j.solmat.2022.112094
Received 22 July 2022; Received in revised form 13 October 2022; Accepted 31 October 2022
Available online 11 November 2022

$(S,Se)_4$ compounds can be maintained up to at least a ratio [Na]/([Na]+[Cu]) = 0.2, which again results in an expansion of lattice parameter [17]. However, the ionic radius of Na is much larger than Cu, so that Na predominantly resides at GB instead of forming alloys [9,18]. The use of soda lime glass (SLG) substrates – which contains considerable amounts of Na – leads to Na incorporation into the absorber due to the high processing temperatures during annealing [13]. Na coming from the substrate was found to prevent Li-alloying via a Li–Na ion exchange process between absorber and substrate, with Na diffusing to the absorber while Li migrates to the glass substrate [11]. Therefore, most groups started implementing either an alkali diffusion barrier or using a Na-free substrate to prevent Li–Na ion exchange, which however eliminates the aforementioned potentially beneficial effects coming from Na incorporation [6,11,12].

Here, the effects of Li incorporation and Na doping are sought to be combined to yield high-performance CZTSSe solar cells. As a matter of simplification, the herein reported approach will be referred to as Li–Na co-doping, even though alloying can occur under our experimental conditions. The combination of alkali elements in CZTSSe absorbers is not per se new and Mule et al. found maximum power conversion efficiency in their material when combining Na and K [19]. Here, we want to investigate in a systematic manner the effect of alkali doping/alloying in $Cu_2ZnSn(S,Se)_4$ using Li and Na. We synthetize CZTSSe absorbers by annealing of spin-coated precursor layers with varying alkali contents in the precursor solution. This vacuum-free layer deposition process combines cost-effectiveness with feasibility for scale-up with regard to commercial production [20]. We study the influence of the combined Li and Na alkali doping strategy on the absorber morphology and relate the alkali concentration in the precursor film to the resulting alkali composition in the absorber. The alkali incorporation into the absorbers is discussed in the light of changes in lattice parameter and of bandgap measurements and J-V characterization is performed to investigate the effect of Li–Na co-doping on the optoelectronic properties.

2. Methods

Samples were prepared on 1 mm thick 5 × 5 cm^2 SLG substrates, on which 200–300 nm SiO_x alkali diffusion barrier was sputtered followed by the deposition of ~800 nm of molybdenum via DC-sputtering. The alkali diffusion barrier is meant to prevent excessive Na in-diffusion and Li–Na ion exchange between the absorber and the SLG substrate. Absorber precursor solutions were prepared with 0.56 M of copper dichloride dihydrate ($CuCl_2{\cdot}2H_2O$, ≥99.95%, Sigma Aldrich), 0.44 M of zinc chloride (ZnCl anhydrous, 99.95%, Alfa Aesar) and 0.50 M of tin chloride dihydrate ($SnCl_2{\cdot}2H_2O$, 98.0–103.0%, Alfa Aesar) dissolved in dimethyl sulfoxide (DMSO, ≥99.9%, Sigma Aldrich). 1.847 M of thiourea (CH_4N_2S, ≥99.0%, Sigma Aldrich) was added acting as coordinating agent. Lithium chloride (LiCl anhydrous, 99%, Fluka) and sodium chloride (NaCl, 99.8%, Roth) were added directly to the precursor solution in various amounts in the range of 0–0.5 M. The compositions were chosen to cover the relevant ranges identified in earlier works for both Li and Na [12,13,21]. The absorber fabrication is depicted in Fig. 1. The precursor solution was spin coated onto the Mo layer, after which the DMSO solvent of the solution was evaporated on a hotplate at 320 °C in air. The process is repeated 10 times to yield a precursor layer thickness of ~1.5 μm. Then the substrates were cut into 4 quarters each, which were annealed in a rapid thermal processing furnace (RTP Annealsys AS ONE 150) inside a semi-tight graphite box with ~800 mg of selenium shots (Se amorphous, 99.999+%, Alfa Aesar). The temperature profile consisted of two plateaus of 15 min each at 350 °C and 540 °C, respectively. Heating rates were set at 1 K/min and the annealing environment was 500 mbar N_2. After selenization, the absorbers were immersed in a 10 wt% aqueous potassium cyanide (KCN, 97+%, Alfa Aesar) solution for 30 s in order to clean the surface from Cu-rich secondary phases. Chemical bath deposition was then used to deposit ~50 nm of CdS buffer layer followed by sputtering of 70 nm and 250 nm of i-ZnO and Al:ZnO, respectively. The top grid consisted of e-beam evaporated 50 nm Ni and 4000 nm Al. Each sample was eventually finalized into 9 cells by mechanical scribing, with an approximate area of 0.30 cm^2 each.

Scanning electron microscope (SEM) measurements were done on a Hitachi S-4800 electron microscope. A time-of-flight secondary ion mass spectrometry (ToF-SIMS) system from ION-TOF was used to measure depth profiles using O^{2+} primary ions with 2 keV ion energy, a current of ~650 nA and a sputter crater size of 300 × 300 μm^2. An area of 100 × 100 μm^2 was analyzed by Bi^+ ions with 25 keV of ion energy. J-V characterization was performed under standard test conditions (100 mW cm^{-2}, 22 °C, AM1.5G solar spectrum) using a solar simulator calibrated with a certified Si diode. A chopped white light source (900 W halogen lamp) with a LOT MSH-300 monochromator was used to record external quantum efficiency (EQE) spectra. The setup was calibrated with certified Si and Ge diodes. The band gap was determined from the EQE spectra using the derivative method. X-ray diffraction (XRD) patterns were recorded in $2\theta/\theta$ scan using a Bruker D8 diffractometer with Cu Kα radiation (λ = 1.5418 Å, beam voltage = 40 kV, beam current = 40 mA), a step size of 0.05°, a scan rate of 0.5 s/step and an incident beam size of 2 mm. For the high-resolution pattern, a step size of 0.005° and a scan rate of 2 s/step were used instead. From the peak positions of the XRD diffraction pattern, θ, the interplanar distance d was calculated using Bragg's law:

$$n\lambda = 2d \bullet \sin(\theta) \tag{1}$$

where n is the diffraction order and λ is the wavelength of the incident radiation. In the tetragonal crystal system, the lattice parameters a and c can be expressed as:

$$\frac{1}{d^2} = \frac{h^2 + k^2}{a^2} + \frac{l^2}{c^2} \tag{2}$$

where h, k, l are the Miller indices of the corresponding crystal planes. In this work we looked at the 400 reflection showing at about θ = 65.8°, from which the lattice parameter a is computed.

3. Results and discussion

SEM cross-section images of co-doped CZTSSe absorbers are shown in Fig. 2. In the upper row (a-e), absorbers with increasing Li solution concentrations are shown from left to right with a Na solution

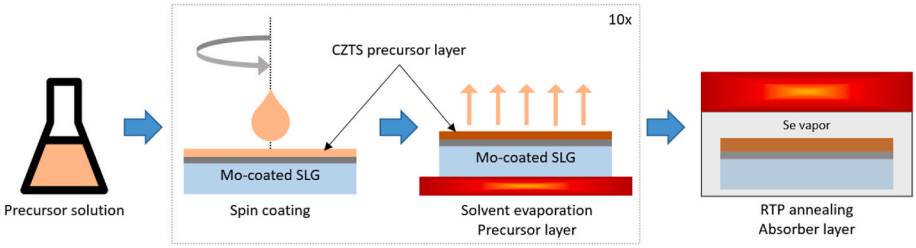

Fig. 1. Sketch of the fabrication process starting from the precursor solution to the absorber layer.

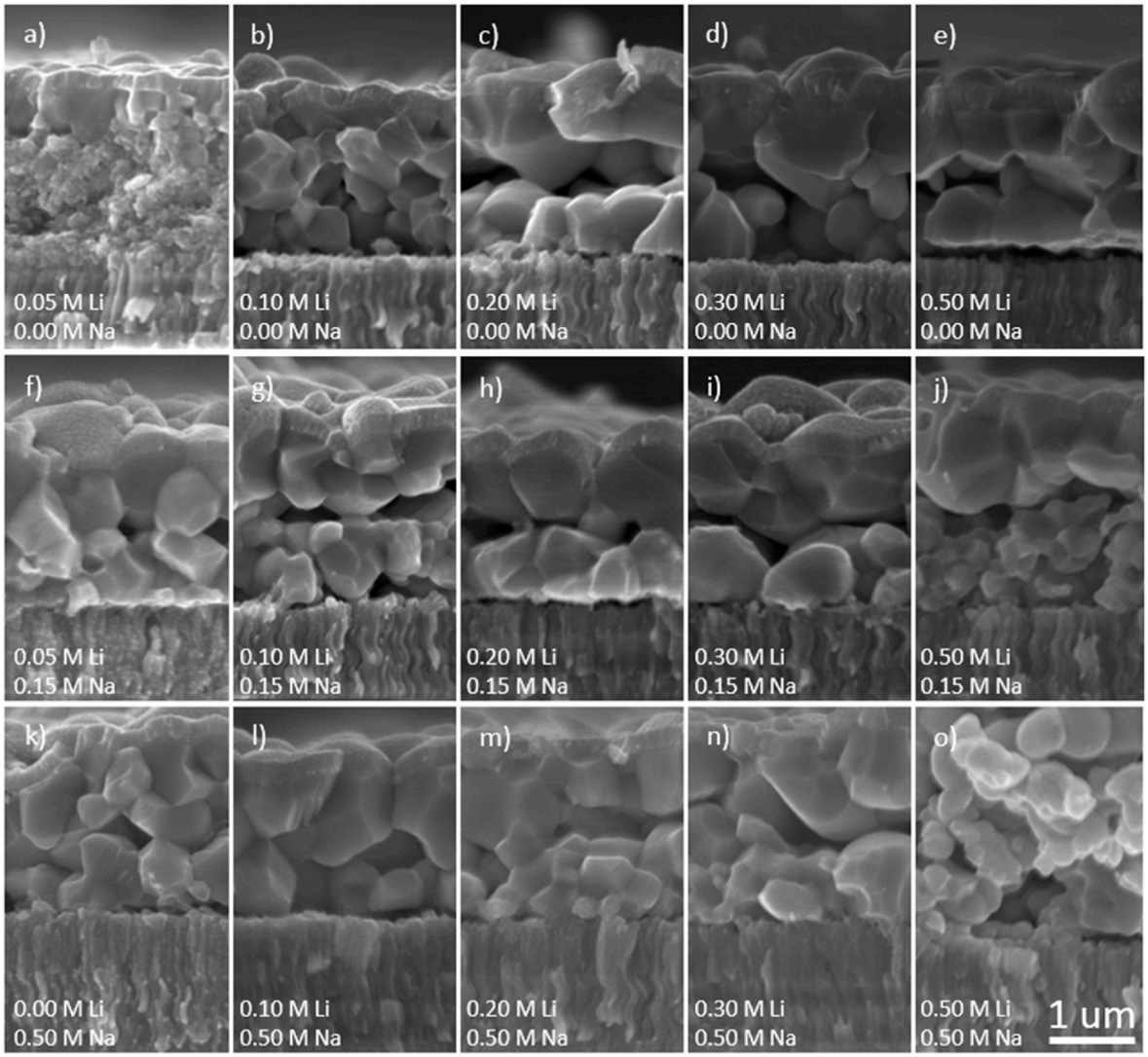

Fig. 2. Cross section SEM of co-doped solar cells, with indicated precursor composition. The top row (a–e) shows samples with increasing Li concentration and fixed Na precursor solution concentration of 0.00 M. The Li concentrations are as follows: a) 0.05 M, b) 0.10 M, c) 0.20 M, d) 0.30 M, and e) 0.50 M. The middle row (f–j) shows samples with increasing Li concentration and fixed Na precursor solution concentration of 0.15 M. The Li concentrations are as follows: f) 0.05 M, g) 0.10 M, h) 0.20 M, i) 0.30 M, and j) 0.50 M. The bottom row (k–o) shows samples with increasing Li concentration and a fixed Na precursor solution concentration of 0.50 M. The Li concentrations are slightly different as the other rows: k) 0.00 M, l) 0.10 M, m) 0.20 M, n) 0.30 M, and o) 0.50 M.

concentration of 0.00 Na, henceforth referred to as *nominally Na free*. In the middle row (f-j), absorbers with increasing Li solution concentrations are shown from left to right with a Na solution concentration of 0.15 Na, henceforth referred to as *low Na*. The bottom row (k-o) shows increasing Li solution concentrations for a Na solution concentration of 0.50 Na, henceforth referred to as *high Na*. The *nominally Na free* series shows improving morphology with increasing Li concentration, characterized by larger grains and less porosity. The *low Na* series shows a comparable trend, but when increasing the Li concentration in solution up to 0.50 M, the morphology shows signs of deterioration. The *high Na* series shows a similar dependency of the morphology on the Li content, even though the onsets for both morphology improvement and deterioration seem to appear at lower Li solution concentrations. The morphology improvement upon Li addition stands in accordance with previous studies, which attributed it to the formation of Li_xSe phases, exerting a fluxing effect on the forming absorber [12]. The morphology deterioration has been explained by Cabas Vidani et al. on nominally Na free absorbers by inhomogeneous distribution of Li compounds in the precursor film, as LiCl does not form sulfide complexes with thiourea, eventually leading to the formation of dendritic features at high nominal Li concentrations [12,22]. Here, the *nominally Na free* absorbers do not show significant morphology deterioration, most likely because the relevant Li concentrations are not reached. For the *low Na* and *high Na* series, however, the suggested mechanism can be expected to be applicable. As neither LiCl, nor NaCl form sulfide complexes with thiourea, excessive NaCl concentration in the precursor solution could also results in inhomogeneous distribution [22]. As a consequence, the onset for morphology worsening might be reached at lower nominal Li concentration when increasing the nominal Na concentration. Nonetheless, good morphology can be obtained for all investigated Na concentrations. This is remarkable as these results point towards a broad process window for favorable microstructure. Finally, we also point out that the back contact layer is considerably thicker for the *high Na* series (~1.6 μm) in comparison to the other series (~1.2 μm). This thickening can be partly gathered from Fig. 2 and is shown in more detail in Table S1 in Supplementary Material. We assign it to the increased $MoSe_2$ layer thickness in the *high Na* series, which probably stems from the catalytic activity of Na favoring $MoSe_2$ formation, which has been reported for CIGS and is hence assumed to be applicable for CZTSSe as well [23].

Fig. 3 shows elemental depth profiles recorded by ToF-SIMS of a co-

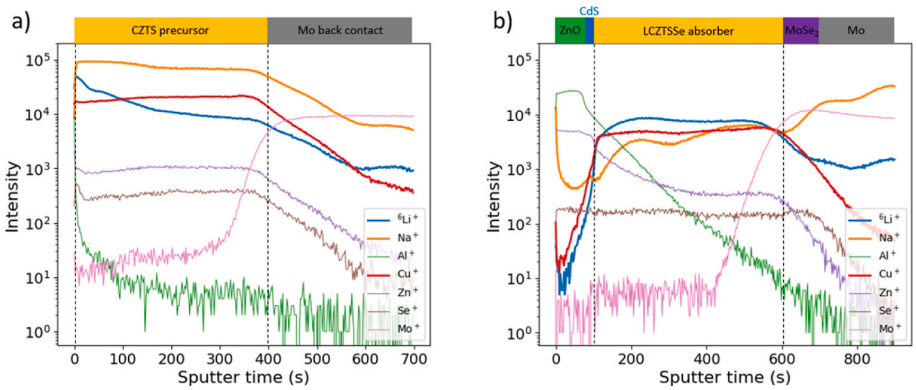

Fig. 3. Representative ToF-SIMS depth profile of a co-doped absorber (0.15 M Na, 0.20 M Li), (a) as precursor layer, and (b) after RTP annealing and completion into solar cell. The indicative layer structure is shown on top.

doped absorber of the *low Na* series (0.15 M Na) with a nominal Li concentration of 0.20 M (a) before, and (b) after annealing. The absorber layer is marked with an orange bar and vertical dashed lines. The lower limit of the absorber layer is determined as 50% of the maximum Cu^+ count value and the upper limit of the absorber layer is determined as 50% of the maximum Mo^+ count value. In order to compare different absorbers with each other, the relevant counts (here: $^6Li^+$ and Na^+) were averaged over the absorber layer. This number was then normalized by the average of the Cu^+ counts over the absorber layer. The resulting ratios are summarized in Fig. 4. The upper row shows the relative Li and Na concentrations in the precursor layer before annealing as a function of nominal Li concentration in the solution. On the one hand, the Li concentration in the precursor layer increases with increasing nominal Li concentration. On the other hand, the Na concentration in the precursor layer is not affected by changes to the Li concentration in solution. As expected, the Na level is higher for the *high Na* series than for *the low* Na series. Thus, the alkali concentrations in the precursor layer are within expectations. ToF-SIMS profiles of the *nominally Na free* series before annealing could not be obtained due to technical reasons.

Fig. 4c-d shows the relative Li and Na concentrations in the absorber layer (after annealing) as a function of nominal Li concentration. The increase in $[^6Li^+]/[Cu^+]$ ratio with increasing nominal Li concentration is partially maintained, even though a clear saturation is reached for high nominal Li concentrations. The onset for saturation occurs at a nominal Li concentration of 0.3 M for both the *low Na* and the *nominally Na free* series, and 0.2 M for the *high Na* series, respectively. Not only does excessive Li result in saturation of Li content, but also presence of high nominal Na concentration induces this behavior at lower Li concentration. The same was observed in terms of morphology degradation (Fig. 2). The latter has been explained by inhomogeneous Li distribution due to the inability of LiCl to form sulfide complexes with thiourea resulting in Li-containing dendritic features. The formation of the plateau in Fig. 4c could be assigned to the same mechanism. We believe that excessive initial Li concentrations result in the formation of Li-rich dendritic features, whose Li content is ultimately lost and not incorporated into the absorbers. Hence, the maximum practical Li concentration in the absorber is determined by the appearance of these features resulting in a self-limiting Li incorporation process. It is closely correlated with degradation of the morphology.

The overall Li absorber concentration is higher, the less nominal Na

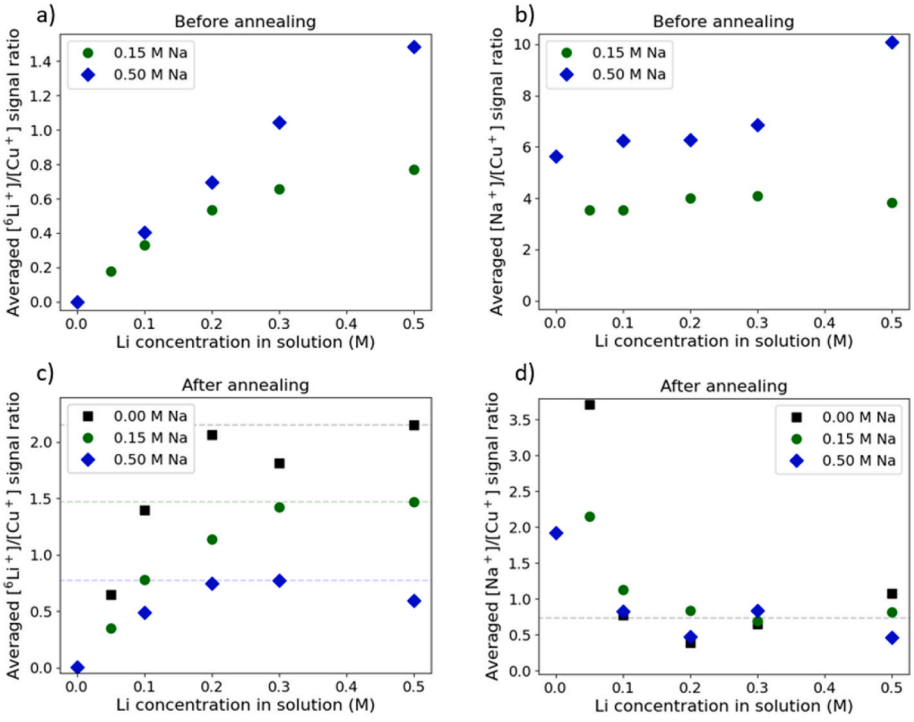

Fig. 4. *Relative SIMS signal ratios $^6Li^+/Cu^+$ and Na^+/Cu^+ averaged over the absorber depth, as function of the initial Li concentration in the precursor solution. The top row shows the (a) Li and (b) Na signal ratios to Cu for selected precursor layers. The bottom row shows the (c) Li and the (d) Na signal ratios to Cu for selected absorber layers. Profiles of precursor layers of* nominally Na free *series could not be obtained for technical reasons. The dashed lines visualize saturation of the respective concentrations in subfigures (c) and (d).*

is added to the precursor solution (*nominally Na free* > *low Na* > *high Na*). Fig. 4d shows a large reduction in Na inside the absorbers when nominal Li concentration is increased, resulting in saturation at low Na levels. This behavior is independent of the nominal Na concentration in the precursor solution. Consequently, we observe a mutual dependency of Li and Na: the final alkali concentrations of Li and Na depend on the initial concentration of both. A possible model explaining this mutual dependency is the competition for same lattice sites. Both Li and Na are known to easily occupy Cu- or Zn-sites, with the former more likely being vacant and available for alkali occupation in a Cu-poor composition as it is the case here [9,24,25]. Yet, Na predominantly remains at GB, due to the radius mismatch of Na^+ compared to Cu^+ and Zn^{2+} and the larger predicted substitution energy of Na_{Cu} as compared to Li_{Cu} (0.64 eV vs. 0.25 eV) [9]. Hence, mutual dependency most probably stems from another mechanism. We propose a second model, based on the formation of alkali selenide phases acting as fluxing agents during annealing. As the enthalpies of formation of Li_2Se and Na_2Se are both similarly exothermic [26], the difference in alkali abundancy in the precursor layer is expected to determine the concentrations of the alkali selenide phases. The increasing presence of one alkali element offers a statistical advantage over the other alkali element to capture Se atoms and to form selenides. Therefore, the presence of both Li and Na creates a mutual restriction of the respective selenide phases. The alkali selenide phases then (partially) take over the role of Cu_xSe, which is an intermediate phase in the formation route of the $Cu_2ZnSnSe_4$ compound, as proposed by Fella et al. [27].

$$(Cu, Li, Na), Zn, Sn \xrightarrow{\sim 190\ ^\circ C} (Cu, Li, Na)_x Se \xrightarrow{\sim 420\ ^\circ C} Cu_2ZnSnSe_4$$

The beneficial fluxing effect of either alkali selenide phases provides Se to the material during synthesis of the CZTSSe phase. The remaining alkali elements are then implanted into the material, as it would occur for Cu originating from Cu_xSe. Therefore, the ratio of the alkali selenide concentration could translate into a mutual dependency of the respective elements in the absorber.

Another aspect visible from the ToF-SIMS analysis is how much the Na concentration is reduced upon annealing (Fig. 4b vs. Fig. 4d), especially in presence of Li. One possible explanation for this observation is Na uptake by the Mo back contact. Comparing Fig. 3a with Fig. 3b, it can be seen that the Na counts are strongly increased within the metal Mo back contact after annealing, while the same is not observed for Li. The Mo back contact might act as a sink for Na – and possibly as a reservoir simultaneously – and participates in the equilibrium Na concentration by storing excess or donating Na to the absorber. It remains unclear, whether Na in the Mo back contact is provided only from the absorber or also from the gas phase or even from the SLG substrate. The latter would point towards a leaky SiO_x diffusion barrier layer. In any case, Mo acting as Na sink/reservoir would explain the saturation of the Na content as observed in Fig. 4d. Another contributing factor for the strong reduction in Na concentration may be related to its entry into the gaseous phase during annealing, before being lost in the semi-tight reactor [28]. Grain size effects might additionally contribute to the lowering in Na concentration upon annealing. All the discussed effects could also explain the weak Na-gradient in CZTSSe layer observed in Fig. 3.

Finally, the Na levels in all the absorbers – whether the precursor solution contained Na or not – are very close to each other (especially when Li $\geq$ 0.1 M, see Fig. 4d). This is remarkable, as it suggests that the SLG substrate provides almost as much Na to the absorber as direct Na addition to the precursor solution. Consequently, the SiO_x alkali diffusion barrier, which has been introduced in previous studies [6,12], does not fully limit Na incorporation, making absorber fabrication potentially less reproducible because of variations in substrate composition and/or annealing temperature. Given the mutual dependency of Na and Li in the absorber, this uncertainty could even reflect in the final Li absorber concentration. Yet, the alkali diffusion barrier does prevent the Na–Li ion exchange mechanism as reported by Cabas Vidani et al. [11,12] Thus, we speculate that Na of the SLG substrate diffuses through the Se vapor during annealing in form of Na_xSe and represents a significant share of the Na ultimately incorporated in the absorber, as also claimed by Abzieher et al. [29] It stands in accordance with our proposed model for the mutual dependency of Li and Na in CZTSSe absorbers as the alkali element incorporation is suggested to depend on the formation of Na_xSe and Li_xSe during annealing.

We then sought to discriminate between incorporation of alkali elements in the bulk or at GB by its impact on lattice parameter and on the band gap. Fig. 5a shows the lattice parameter *a* calculated from the 400 XRD reflection. The statistical relevance of our reported lattice parameter values was confirmed by an estimation of the experimental uncertainty based on error propagation calculations of the standard deviation of the 110 Mo peak position (Supporting Material). The black dashed lines indicate the maximum and minimum lattice parameter values for absorbers from the *nominally Na free* series. The lattice parameter *a* increases in all series when adding more Li to the solution before reaching saturation for high nominal Li, with the *high Na* series reaching slightly larger values than the *low Na* series. All co-doped absorbers show larger lattice parameters than the minimum value set by the *nominally Na free* series. Nevertheless, the maximum values – also set from the *nominally Na free* series – is not overcome significantly by either of the co-doped absorber series. The increase in lattice parameter *a* as a function of nominal Li concentration stems from Li occupying V_{Cu} in the CZTSSe lattice, which were left vacant in the Cu-poor composition. Li–Se has a slightly different bond valence parameter compared to the Cu–Se bond valence parameter resulting in a change in lattice parameter *a* [12]. Other influences on the lattice parameter *a* were considered but subsequently ruled out. Differences in the S/Se ratio would affect both lattice parameters *a* and *c* equally and would reflect in a shift of the 112 XRD peak according to Vegard's law [30,31]. Based on the XRD diffraction patterns presented in Fig. S1 in Supplementary Material, neither does *c* show any comparable trend as *a*, nor is the 112 peak shifted, with the 112 peak position lying at around 27.27° for all the absorbers corresponding to S/(S + Se) ≈ 5%. This estimation is based on Vegard's law with the 112 peak position for $Cu_2ZnSnSe_4$ and Cu_2ZnSnS_4 being at 27.2° and 28.5, respectively [32,33]. Another possibility is a changed state of Cu/Zn disorder, but this would mainly affect lattice parameter *c* instead of *a* [34]. Eventually, increasing Cu deficiency could also influence the lattice parameters via excessive V_{Cu} formation. But again, this would mainly affect lattice parameter *c* [35]. Furthermore, we did not see any significant variations in the Cu/Zn ratio from XRF measurements. As a matter of completion, there is a possibility that some or all of the aforementioned mechanisms occur together, but balance out each other's effects on the lattice parameters. This cannot be ruled out, but it leaves alloying as the more likely mechanism. Therefore, the trend of increasing lattice parameter *a* with increasing Li content confirms the occurrence of Li-alloying despite the presence of Na, most likely because the SiO_x alkali diffusion barrier is enough to prevent Li–Na ion exchange. The saturation in lattice parameter *a* reached for all series at high Li concentration could be related to the self-limiting Li incorporation process proposed from the ToF-SIMS depth profile analysis (Fig. 4c). That is, the onset for saturation of the lattice parameter *a* occurs at comparable nominal Li concentrations as concentration saturation from ToF-SIMS data. It is remarkable that most absorbers are located somewhere in between the minimum and maximum values set by the *nominally Na free* series despite containing similar Li amounts. The co-doped absorbers of the *low Na* series and *high Na* series with the lowest Li concentration lie well above the minimum value. Since the *high Na* series includes an absorber without any Li and it still shows larger *a* values than the Li-alloyed minimum value, the lattice parameter *a* must also be influenced by Na. The observation that the lattice parameter *a* of *high Na* co-doped absorbers is larger than for the *low Na* absorbers despite lower Li content, supports this claim. The anticipated mechanism is Na-alloying, and is analogous to Li-alloying. Even though the ionic radii of Cu and Na do not match and Na predominantly remains at

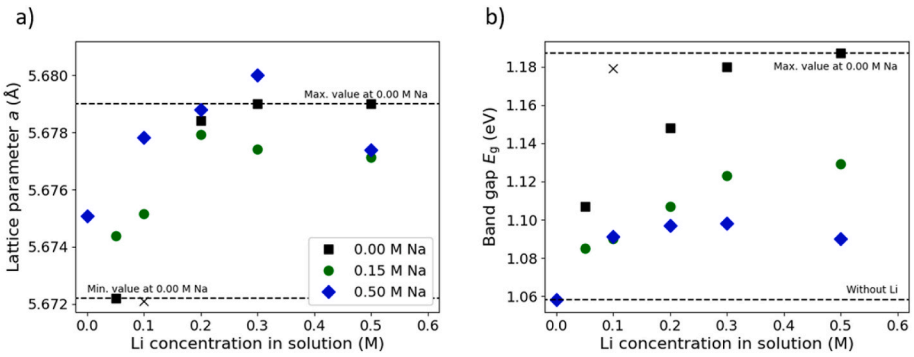

Fig. 5. a) Lattice parameter a for co-doped absorbers with Na concentration in the precursor solution of 0.00 M (black squares), 0.15 M (green dots) and 0.50 M (blue diamonds). The black dashed lines mark the maximum and minimum values, respectively. b) Band gap values obtained from EQE spectra via the derivative method. The cross marks a data point flagged as an outlier. The black dashed lines refer to the minimum band gap value and the maximum band gap value, respectively. The legend is valid for both subplots. The XRD and EQE data are presented in the Supplementary Material. (For interpretation of the references to color in this figure legend, the reader is referred to the Web version of this article.)

GB, some Cu-sites are known to be occupied by Na [14,17]. The bonding distance between Na and Se is even larger than between Li and Se [10], so that the incorporation of Na ions distorts the lattice more heavily. Yet, the number of incorporated Na is very likely to be lower than in the Li-alloying case, due to the higher substitution energy mainly [9]. This is bolstered by the observation that the lattice parameter *a* of co-doped absorbers from the *high Na* series only matches the maximum value obtained from *nominally Na free* series, but does not overcome it drastically. This is surprising, because the *high Na* absorbers contain Li and Na, which both contribute to an increase of the lattice parameter *a*, so that further increase in *a* could have been anticipated. Two possible explanations for this observation are presented. First, Li-alloying could be hindered to some extent under the presence of Na, so that Li remains present, but is not incorporated into the lattice. Second, the mutual dependency discussed before might directly influence the degree of alloying of both elements, so that the increase in lattice parameter *a* is limited. It remains unclear, which of the two mechanisms is responsible for the reported behavior and a combination of both cannot be ruled out. In any case, as the XRF measurements showed a Cu/(Zn + Sn) ratio in the region of 0.75–0.79, and the relative concentration of Li and Na can be estimated to be below 10% and 1%, respectively, with respect to Cu based on the alkali concentration in the precursor solution [12,21] all samples remain Group-I-poor.

Fig. 5b shows the band gap (E_g) values obtained from EQE spectra via the derivative method. Again, the results are put into perspective to the values of the *nominally Na free* series. The only Li-free absorber was marked as the lower reference value (black dashed line). The upper reference value refers to the maximum band gap obtained from the *nominally Na free* series. All the band gap values of the co-doped absorbers are somewhere between the lower and the upper reference values and none of them reaches the maximum value. The band gap values are influenced by both alkali element concentrations. On the one hand, increasing nominal Na concentration results in lower band gap values (*nominally Na free* > *low Na* > *high Na*). On the other hand, there is an almost linear increase in E_g as a function of Li concentration in the precursor solution. This dependency is stronger the less Na is added to the solution. Saturation of E_g is reached at high nominal Li concentration for all the series. The increase in band gap as a function of Li has been reported before by Cabas Vidani et al. and was ascribed to Li-alloying of the CZTSSe phase, as the pure Li phase ($Li_2ZnSnSe_4$) shows a band gap of about 2.0 eV [12,36]. Other mechanisms potentially responsible for the changes in band gap such as the aforementioned differences in S/Se ratio or a different state of Cu/Zn disorder were ruled out due to the missing effect on the lattice parameters. Moreover, the trends of lattice parameter and band gap and our proposed model of alloying are very consistent with each other. From the observation that the band gap values are lower the more Na was added to the solution, we conclude that Na does not per se increase the band gap in our absorbers, despite the Li-like influence on the lattice parameter a. Despite recent reports stating a band gap decrease in CZTSSe absorbers upon Na addition, it is unlikely in our case, as it would require Na to be implanted interstitially into the lattice [37,38]. It is, however, more likely for Na being incorporated into Cu-sites, because the occupation energy of Na_i is considerable higher than Na_{Cu} or even Na_{Zn} [9]. The substitution mechanism also better fits the changes in lattice parameter *a* observed before. As a consequence, the apparent influence of Na on the band gap most probably stems from the influence of Na on Li. Either, Na actually prevents Li-alloying or it simply influences the abundancy of Li in the absorber via the mutual dependency of the alkali elements. That is, the presence of Na reduces the overall availability of Li, so that the ratio of Li-alloyed phase is in any case lower, the more Na there is. As only the Li-alloyed phase seems to significantly contribute to the band gap increase, we can also explain, why none of the co-doped absorbers reaches the upper reference band gap value. It emphasizes the need for a reliable barrier against Na coming from the substrate, to rule out the influence of slight composition variations in the SLG substrate on the degree of alloying in the absorber. But, in spite of Na influencing Li-alloying, we show that the band gap increases with increasing Li concentration in co-doped absorbers. Consequently, Li-alloying is still taking place despite the Na presence, supporting the claims derived from the lattice parameter interpretation. No Li-free samples are presented for the *nominally Na free*, and the *low Na* series, due to their resemblance in determined parameters to a recently reported sample by Cabas Vidani et al., which can be considered as nominally Na free, because of identical fabrication methods [12]. Therefore, no significant variation can be expected for a Li-free absorber in the *low Na series*.

Finally, the influence of Li–Na co-doping in solution-based CZTSSe absorbers on PV performance is studied. Fig. 6 shows the optoelectronic properties – V_{oc}, short-circuit current (J_{sc}), fill factor and power conversion efficiency (PCE) – as boxplots. The *nominally Na free* series shows an increase in V_{oc} with increasing Li concentration. At the upper end of the Li concentration range, the PCE is limited as a result of fill factor deterioration. The *low Na* series shows slightly higher V_{oc} and J_{sc} at low Li concentrations compared to the *nominally Na free* series. However, similar deterioration of the fill factor is observed in the *low Na* series, even though the onset occurs at lower Li concentrations as compared to the *nominally Na free* series. As visible from Fig. 7, specific samples of the *high Na* series suffer from strongly degraded diode properties, which probably originate from a separate issue. The improvement in V_{oc} in the *low Na* series can be assigned to the defect passivating effects of Na, whereas the J_{sc} increase most likely stems from improved interfaces, as it can be gathered from the EQE curves (see Fig. S2 in Supplementary Material). The reduction in fill factor at high alkali concentration has been reported before and was ascribed to layer porosity and inhomogeneous distribution of lithium-containing compounds [12]. We consider this as the most likely mechanism in our samples, as the onset of fill factor deterioration matches well the onset for morphology deterioration match (Fig. 2).

Fig. 7 shows J-V curves of the best cells of the co-doped absorbers. The V_{oc} in the *high Na* series is clearly lowered. This can be partly explained by the worsened morphology and overall smaller grain size in this series. Furthermore, it is visible that R_s tends to increase with

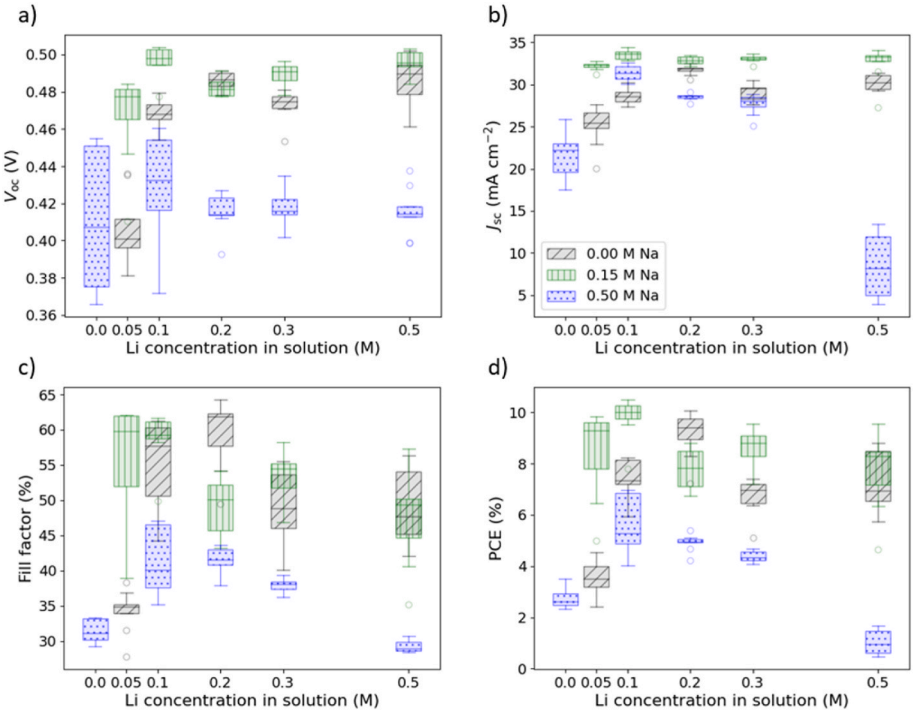

Fig. 6. The open circuit voltage (a), short circuit current (b), fill factor (c) and power conversion efficiency (d) of co-doped absorbers are shown as boxplots as function of Li concentration in the precursor solution. The same legend applies to all subplots. The various Na solution concentrations are indicated by colors and hatches. Each boxplot represents a sample with 9 cells with individual area of about 0.3 cm^2. (For interpretation of the references to color in this figure legend, the reader is referred to the Web version of this article.)

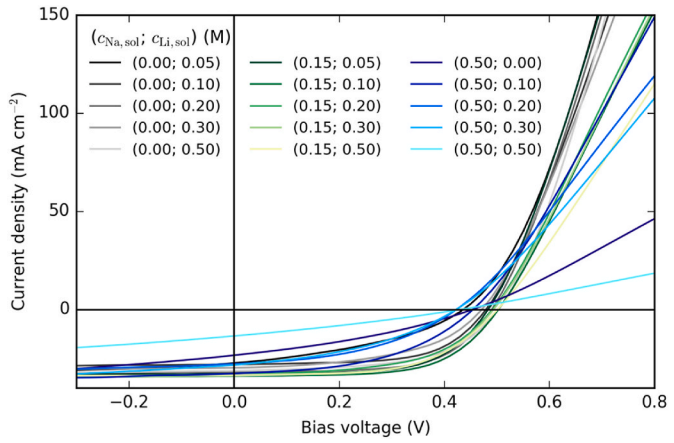

Fig. 7. J-V curves of the best cell of each investigated co-doped absorber sample, with alkali concentrating in the precursor solution indicated in parentheses.

increasing nominal Na concentration. The spread of R_s values within the series also increases with increasing nominal Na concentration (R_s and R_p boxplots can be found in Fig. S3 in Supplementary Material). We assume that R_s deterioration in the *high Na* series stems from the enhanced $MoSe_2$ formation [39]. Moreover, the fill factor of the high Na series seems to be further affected by low shunt resistance, with the reason for that remaining unclear.

An aspect deserving further consideration is the dependency of the optimal Sn concentration on the alkali element type used, as investigated by *Haass* et al. [6] Non-optimized Sn concentrations might lead to secondary phase formation, which could potentially influence series resistance, shunt resistance and more generally device performance. In our work, the Sn concentration was kept constant in all samples, for two reasons. First, the change in optimum Sn concentration in presence of multiple alkali elements was unknown a priori, and second, to limit the scope of our already significant experimental work. Non-optimal Sn concentration may be a factor for the overall lower performances of the *high Na* series. Even though the XRD diffraction patterns provided in Supplementary Material (Fig. S1) do not show signs for drastic formation of secondary phases, the reflexes of most secondary phases in CZTSSe overlay to the ones assigned to the CZTSSe phase. Hence, secondary phases might be present in our films without being evidenced.

Co-doping of CZTSSe absorbers using Li and Na resulted in marginally improved best cell efficiencies (10.5% vs. 10.1% for Li-only reference). The values reported correspond to devices without anti-reflective coating. The modified absorbers benefit from increased V_{oc} and J_{sc}. As all the absorbers might suffer from non-optimized Sn concentration, slight adjustments of the matrix composition may improve PCE even more. Considering the different onsets for morphology deterioration (Fig. 2), it is not so surprising that the best-performing devices for the *nominally Na free* series and low Na series were found at different nominal Li concentrations.

4. Conclusion

As a summary, we established a strategy to incorporate controlled amounts of both Li and Na into CZTSSe absorbers via composition adjustment of the precursor solution. In line with existing reports, the incorporation of Li appears to be self-limiting at high concentrations. Co-doping of CZTSSe absorbers with Li and Na results in a mutual dependency of the concentration of the individual alkali elements. This mutual dependency arises during the CZTSSe absorber synthesis, which we ascribed to a mechanism mediated by the formation of alkali selenide phases. The final alkali concentrations in the absorbers are probably dependent on the specific annealing conditions. Both, Li and Na elements can occupy in-grain lattice sites resulting in alloying impacting lattice parameter and bandgap. Li is favored thanks to the lower substitution energy of Li_{Cu} as compared to Na_{Cu} originating from the ionic radius mismatch between of Cu^+ and Na^+. Yet, Li-alloying remains hindered in presence of Na. Excess amounts of alkali elements result in degradation of the absorber morphology and of PV performances.

As a consequence, band gap tuning by means of Li-alloying is less effective when Na is present in the system. It was found that SLG substrates act as a significant Na source via the gas phase. Achieving a reproducible fabrication process of kesterite absorbers requires control

of all – intentional and unintentional – alkali supply sources. Composition variations in e.g. SLG substrate may well be an overlooked factor affecting the alkali concentrations and performances of CZTSSe absorbers.

Finally, although Li and Na are both known for their highly beneficial effects on CZTSSe-based solar cells, combination of both lead to similar absorber morphologies and only marginally improved optoelectronic properties. Nonetheless, the best cell performance was raised from 10.1% for the Li-only reference to 10.5% upon addition of Na to the precursor solution, as both V_{oc} and J_{sc} were improved in co-doped absorbers as a result of additional defect passivation and improved interfaces.

Funding sources

This project has received funding from the European Union's Horizon 2020 research and innovation programme under grant agreement No 952982.

CRediT authorship contribution statement

S. Moser: Writing – review & editing, Writing – original draft, Visualization, Validation, Methodology, Investigation, Data curation, Conceptualization. **A.N. Tiwari:** Writing – review & editing, Supervision, Funding acquisition, Conceptualization. **R. Carron:** Writing – review & editing, Supervision, Methodology, Funding acquisition, Conceptualization.

Declaration of competing interest

The authors declare that they have no known competing financial interests or personal relationships that could have appeared to influence the work reported in this paper.

Data availability

Raw data is available at https://zenodo.org/communities/custom-art/?page=1&size=20 under DOI 10.5281/zenodo.6880879 (will be published on zenodo as soon as the manuscript is accepted)

Acknowledgement

The Laboratory for Surface Science & Coating Technologies at Empa is gratefully acknowledged for granting access to SIMS and XRD measurements facilities. The Transport at Nanoscale Interfaces Laboratory at Empa is gratefully acknowledged for granting access to SEM measurement facilities.

Appendix A. Supplementary data

Supplementary data to this article can be found online at https://doi.org/10.1016/j.solmat.2022.112094.

References

[1] M.A. Green, E.D. Dunlop, J. Hohl-Ebinger, M. Yoshita, N. Kopidakis, K. Bothe, D. Hinken, M. Rauer, X. Hao, Solar cell efficiency tables (Version 60), Prog. Photovoltaics Res. Appl. 30 (2022) 687–701, https://doi.org/10.1002/pip.3595.

[2] Y.E. Romanyuk, S.G. Haass, S. Giraldo, M. Placidi, D. Tiwari, D.J. Fermin, X. Hao, H. Xin, T. Schnabel, M. Kauk-Kuusik, P. Pistor, S. Lie, L.H. Wong, Doping and alloying of kesterites, J. Phys. Energy 1 (2019), 044004, https://doi.org/10.1088/2515-7655/ab23bc.

[3] Y. Gong, Y. Zhang, Q. Zhu, Y. Zhou, R. Qiu, C. Niu, W. Yan, W. Huang, H. Xin, Identifying the origin of the Voc deficit of kesterite solar cells from the two grain growth mechanisms induced by Sn2+ and Sn4+ precursors in DMSO solution, Energy Environ. Sci. 14 (2021) 2369–2380, https://doi.org/10.1039/d0ee03702h.

[4] M. He, C. Yan, J. Li, M.P. Suryawanshi, J. Kim, M.A. Green, X. Hao, Kesterite solar cells: insights into current strategies and challenges, Adv. Sci. 8 (2021) 1–16, https://doi.org/10.1002/advs.202004313.

[5] A.S. Nazligul, M. Wang, K.L. Choy, Recent development in earth-abundant kesterite materials and their applications, Sustain. Times 12 (2020), https://doi.org/10.3390/su12125138.

[6] S.G. Haass, C. Andres, R. Figi, C. Schreiner, M. Bürki, Y.E. Romanyuk, A.N. Tiwari, Complex interplay between absorber composition and alkali doping in high-efficiency kesterite solar cells, Adv. Energy Mater. 8 (2018) 1–9, https://doi.org/10.1002/aenm.201701760.

[7] H. Xin, S.M. Vorpahl, A.D. Collord, I.L. Braly, A.R. Uhl, B.W. Krueger, D.S. Ginger, H.W. Hillhouse, Lithium-doping inverts the nanoscale electric field at the grain boundaries in Cu2ZnSn(S,Se)4 and increases photovoltaic efficiency, Phys. Chem. Chem. Phys. 17 (2015) 23859–23866, https://doi.org/10.1039/c5cp04707b.

[8] A. Lafond, C. Guillot-Deudon, J. Vidal, M. Paris, C. La, S. Jobic, Substitution of Li for Cu in Cu2ZnSnS4: toward wide band gap absorbers with low cation disorder for thin film solar cells, Inorg. Chem. 56 (2017) 2712–2721, https://doi.org/10.1021/acs.inorgchem.6b02865.

[9] T. Maeda, A. Kawabata, T. Wada, First-principles study on alkali-metal effect of Li, Na, and K in Cu2ZnSnS4 and Cu2ZnSnSe4, Phys. Status Solidi Curr. Top. Solid State Phys. 12 (2015) 631–637, https://doi.org/10.1002/pssc.201400345.

[10] B.E. Brese, M. O'Keefe, Bond-valence parameters for solids.pdf, Acta Crystallogr. B 47 (1991) 192–197.

[11] Y. Yang, L. Huang, D. Pan, New insight of Li-doped Cu2ZnSn(S,Se)4 thin films: Li-induced Na diffusion from soda lime glass by a cation-exchange reaction, ACS Appl. Mater. Interfaces 9 (2017) 23878–23883, https://doi.org/10.1021/acsami.7b07796.

[12] A. Cabas-Vidani, S.G. Haass, C. Andres, R. Caballero, R. Figi, C. Schreiner, J. A. Márquez, C. Hages, T. Unold, D. Bleiner, A.N. Tiwari, Y.E. Romanyuk, High-efficiency (LixCu1-x)2ZnSn(S,Se)4 kesterite solar cells with lithium alloying, Adv. Energy Mater. 8 (2018), 1801191, https://doi.org/10.1002/aenm.201801191.

[13] C.M. Sutter-Fella, J.A. Stückelberger, H. Hagendorfer, F. La Mattina, L. Kranz, S. Nishiwaki, A.R. Uhl, Y.E. Romanyuk, A.N. Tiwari, Sodium assisted sintering of chalcogenides and its application to solution processed Cu2ZnSn(S,Se)4 thin film solar cells, Chem. Mater. 26 (2014) 1420–1425, https://doi.org/10.1021/cm403504u.

[14] S. Giraldo, Z. Jehl, M. Placidi, V. Izquierdo-Roca, A. Pérez-Rodríguez, E. Saucedo, Progress and perspectives of thin film kesterite photovoltaic technology: a critical review, Adv. Mater. 31 (2019), 1806692, https://doi.org/10.1002/adma.201806692.

[15] Haass, S. G., Diethelm, M., Werner, M., Bissig, B., Romanyuk, Y. E. & Tiwari, A. N. 11.2% Efficient Solution Processed Kesterite Solar Cell with a Low Voltage Deficit. Pdf.

[16] M. Werner, C.M. Sutter-Fella, Y.E. Romanyuk, A.N. Tiwari, 8.3% efficient Cu2ZnSn(S,Se)4solar cells processed from sodium-containing solution precursors in a closed reactor, Thin Solid Films 582 (2015) 308–312, https://doi.org/10.1016/j.tsf.2014.10.043.

[17] D. Jiang, Y. Sui, W. He, Z. Wang, F. Wang, B. Yao, L. Yang, Sodium doping of solution-processed Cu2ZnSn(S,Se)4 thin film and its effect on Cu2ZnSn(S,Se)4 based solar cells, Vacuum 184 (2021), 109908, https://doi.org/10.1016/j.vacuum.2020.109908.

[18] J. Kim, G.Y. Kim, T.T.T. Nguyen, S. Yoon, Y.K. Kim, S.Y. Lee, M. Kim, D.H. Cho, Y. D. Chung, J.H. Lee, M.J. Seong, W. Jo, Sodium-Assisted passivation of grain boundaries and defects in Cu2ZnSnSe4 thin films, Phys. Chem. Chem. Phys. 22 (2020) 7597–7605, https://doi.org/10.1039/c9cp06537g.

[19] A. Mule, B. Vermang, M. Sylvester, G. Brammertz, S. Ranjbar, T. Schnabel, N. Gampa, M. Meuris, J. Poortmans, Effect of different alkali (Li, Na, K, Rb, Cs) metals on Cu2ZnSnSe4 solar cells, Thin Solid Films 633 (2017) 156–161, https://doi.org/10.1016/j.tsf.2016.11.027.

[20] K.T. Chaudhary, Thin film deposition: solution based approach, in: A.E. Ares (Ed.), Thin Films, 2021, https://doi.org/10.5772/intechopen.94455. Ch. 10.

[21] M. Werner, C.M. Sutter-Fella, H. Hagendorfer, Y.E. Romanyuk, A.N. Tiwari, Cu2ZnSn(S,Se)4 solar cell absorbers processed from Na-containing solutions in DMSO, Phys. Status Solidi Appl. Mater. Sci. 212 (2015) 116–120, https://doi.org/10.1002/pssa.201431146.

[22] J.C.A. Boeyens, F.H. Herbstein, Ionic complexes of thiourea. II. Chemical and crystallographic survey and determination of the crystal structures of some representative complexes, Inorg. Chem. 6 (1967) 1408–1425, https://doi.org/10.1021/ic50053a027.

[23] X. Zhu, Z. Zhou, Y. Wang, L. Zhang, A. Li, F. Huang, Determining factor of MoSe 2 formation in Cu(In,Ga)Se 2 solar Cells, Sol. Energy Mater. Sol. Cells 101 (2012) 57–61, https://doi.org/10.1016/j.solmat.2012.02.015.

[24] L.E. Oikkonen, M.G. Ganchenkova, A.P. Seitsonen, R.M. Nieminen, Effect of sodium incorporation into CuInSe2 from first principles, J. Appl. Phys. 114 (2013), https://doi.org/10.1063/1.4819105.

[25] D. Shin, B. Saparov, D.B. Mitzi, Defect engineering in multinary earth-abundant chalcogenide photovoltaic materials, Adv. Energy Mater. 7 (2017), 1602366.

[26] Å. Olin, B. Noläng, L. Öhman, E. Osadchii, E. Rosén, Chemical thermodynamics volume 7: chemical thermodynamics of selenium, Chem. Thermodyn. 7 (2005).

[27] C.M. Fella, A.R. Uhl, C. Hammond, I. Hermans, Y.E. Romanyuk, A.N. Tiwari, Formation mechanism of Cu2ZnSnSe4 absorber layers during selenization of solution deposited metal precursors, J. Alloys Compd. 567 (2013) 102–106, https://doi.org/10.1016/j.jallcom.2013.03.056.

[28] J. Sangster, A.D. Pelton, The Na-Se (Sodium-Selenium) system, J. Phase Equil. 18 (1997) 185–189.

[29] T. Abzieher, T. Schnabel, M. Hetterich, M. Powalla, E. Ahlswede, Source and effects of sodium in solution-processed kesterite solar cells, Phys. Status Solidi Appl. Mater. Sci. 213 (2016) 1039–1049, https://doi.org/10.1002/pssa.201532619.
[30] S. Ji, T. Shi, X. Qiu, J. Zhang, G. Xu, C. Chen, Z. Jiang, C. Ye, A Route to Phase Controllable Cu2ZnSn(S1-xSex)4 Nanocrystals with Tunable Energy Bands.Pdf, vol. 3, 2013, p. 2733, https://doi.org/10.1038/srep02733.
[31] S. Adachi, Summary: physical properties of CZTS and CZTSe, in: Earth-Abundant Materials for Solar Cells: Cu2-II-IV-VI4 Semiconductors, 2015, pp. 363–367.
[32] I.D. Olekseyuk, L.D. Gulay, I.V. Dydchak, L.V. Piskach, O.V. Parasyuk, O. V. Marchuk, Single crystal preparation and crystal structure of the Cu2Zn/Cd,Hg/SnSe4 compounds, J. Alloys Compd. 340 (2002) 141–145, https://doi.org/10.1016/S0925-8388(02)00006-3.
[33] S. Schorr, H.-J. Hoebler, M. Tovar, A neutron diffraction study of the stannite-kesterite solid solution series, Eur. J. Mineral 19 (2007) 65–73, https://doi.org/10.1127/0935-1221/2007/0019-0065.
[34] M. Quennet, A. Ritscher, M. Lerch, B. Paulus, The order-disorder transition in Cu2ZnSnS4: a theoretical and experimental study, J. Solid State Chem. 250 (2017) 140–144, https://doi.org/10.1016/j.jssc.2017.03.018.
[35] J. Márquez, M. Neuschitzer, M. Dimitrievska, R. Gunder, S. Haass, M. Werner, Y. E. Romanyuk, S. Schorr, N.M. Pearsall, I. Forbes, Systematic compositional changes and their influence on lattice and optoelectronic properties of Cu2ZnSnSe4 kesterite solar cells, Sol. Energy Mater. Sol. Cells 144 (2016) 579–585, https://doi.org/10.1016/j.solmat.2015.10.004.
[36] A. Weiland, J. Zhang, D.J. Clark, J.A. Brant, Correction: infrared nonlinear optical properties of lithium-containing diamond-like semiconductors Li2ZnGeSe4 and Li2ZnSnSe4, Dalton Trans. 2015 (44) (2017) 11212–11222, https://doi.org/10.1039/C5DT01635E. Dalt. Trans. 46, 10102–10104 doi:10.1039/c7dt90127e.
[37] Z.Y. Zhao, X. Zhao, First-principles study on doping effects of sodium in kesterite Cu 2ZnSnS4, Inorg. Chem. 53 (2014) 9235–9241, https://doi.org/10.1021/ic5013268.
[38] Z. Laghfour, S. Aazou, M. Taibi, G. Schmerber, A. Ulyashin, A. Dinia, A. Slaoui, M. Abd-Lefdil, Z. Sekkat, Sodium doping mechanism on sol-gel processed kesterite Cu2ZnSnS4 thin films, Superlattice. Microst. 120 (2018) 747–752, https://doi.org/10.1016/j.spmi.2018.05.018.
[39] S. Ge, H. Xu, S.N. Khan, W. Yang, R. Hong, Y. Mai, E. Gu, X. Lin, G. Yang, A universal and facile method of tailoring the thickness of Mo(sx,Se1-x)2, contributing to highly efficient flexible Cu2ZnSn(S,Se)4 solar cells, Sol. RRL 5 (2021) 1–9, https://doi.org/10.1002/solr.202100598.